Title: Estimating body segment parameters from three-dimensional human body scans

Authors: Pawel Kudzia[12], Erika Jackson[2], Genevieve Dumas[2]

Affiliations:

[1] Simon Fraser University, Department of Engineering Science, Burnaby, BC, Canada

[2] Queen's University, Department of Mechanical and Material Engineering, Kingston, ON, Canada

Corresponding author:

Pawel Kudzia, M.A.Sc., B.Eng

Department of Engineering Science

Shrum Science Centre K9625

8888 University Drive

Burnaby, BC V5A 1S6, Canada

Email: pawel.kudzia5@gmail.com

Twitter: @PKudzia_BioMech

Competing Interests: None

Abstract word count: 297

Manuscript word count: 5222

Figures: 8

Tables: 6

Abstract

Body segment parameters are inputs for a range of applications. The estimation of body segment parameters that are participant-specific is desirable as it requires fewer prior assumptions and can reduce outcome measurement errors. Commonly used methods for estimating participant-specific body segment parameters are either expensive and out of reach (medical imaging), have many underlying assumptions (geometrical modelling) or are based on a specific subset of a population (regression models). Our objective was to develop a participant-specific 3D scanning and body segmentation method that estimates body segment parameters without any assumptions about the geometry of the body, ethnic background, and gender, is low-cost, fast, and can be readily available. Using a Microsoft Kinect camera, we developed a 3D surface scanning protocol that estimated participant-specific body segment parameters. To evaluate our system, we performed repeated 3D scans of 21 healthy participants (10 male, 11 female). We used open-source software to segment each body scan into 16 segments (head, torso, abdomen, pelvis, left and right hand, forearm, upper arm, foot, shank and thigh) and wrote custom software to estimate each segment's mass, mass moment of inertia in the three principal orthogonal axes relevant to the center of the segment, longitudinal length, and center of mass. We compared our body segment parameter estimates to those obtained using two comparison methods and found that our system was consistent in estimating total body volume between repeated scans (male $p=0.1194$, female $p = 0.2240$), estimated total body mass without significant differences when compared to our comparison method and a medical scale (male $p=0.8529$, female $p = 0.6339$), and generated consistent and comparable estimates across all of the body segment parameters of interest. The work here outlines an inexpensive 3D surface scanning approach for estimating a range of participant-specific body segment parameters.

Keywords: body segment parameters, 3D scanning, inertial parameters, anthropometrics, biomechanics

Introduction

Body segment parameters (BSPs) are required inputs for a range of applications in biomechanics. BSPs include the masses of body segments, the positions of the center of mass of body segments with respect to a segment reference frame, segmental mass moments of inertia with respect to a segment point, and body segment lengths. BSPs can serve as input data for engineering prosthetics (1,2), for ergonomic design (3), and are required for inverse dynamics (4). Although 'generic' datasets that are composed of measurements from a range of humans can be used for approximating BSPs of people, direct *in vivo* participant-specific estimates provide the highest level of accuracy (5). Unfortunately, direct approaches to estimate BSPs can be cumbersome and expensive. In this work, we developed and evaluated an easy-to-implement method for indirectly estimating participant-specific BSPs using an inexpensive consumer depth camera.

Participant-specific BSPs reduce errors associated with biomechanical outcome measures. BSPs estimates can be sensitive to the morphology, age, and gender of a person (6,7). In inverse dynamics analysis, small variations in the BSP inputs can result in clinically significant differences in the outcomes measures (8–11). Depending on the method used to estimate BSPs, there may be large discrepancies in multiple of the BSPs estimates, further increasing error in the outcome measures (12). Representative BSP estimates are especially important in open-chain or high acceleration motion, such as running and jumping, where there are large body segment accelerations, and in airborne movements, where there are no external forces (13). Populations that have less available data for making approximations using 'generic' datasets, such as pregnant women (14), amputees (15), and children (6), will benefit the most from the use of participant-specific BSPs on outcome measure accuracy.

To estimate BSPs requires both density estimates and geometric properties. Medical imaging is the gold standard approach for estimating density. Magnetic resonance imaging (16,17) and computed tomography have been used to estimate *in vivo* BSPs of people by estimating both the geometric and density profiles of the individual body segments (18). The limitations are that there is exposure to low dose radiation for CT scanning approaches, medical imaging incurs high costs, and for certain populations, these approaches may not be feasible (e.g., pregnant women and children) (6). Dual-energy x-ray absorptiometry has also shown potential in this field (15) as it is less expensive and faster than the aforementioned approaches. But in general, medical imaging is not readily available and is largely impractical for many laboratory-based experiments seeking inexpensive and minimally involved methodologies.

Indirect methods are a common approach used for estimating participant-specific BSPs. One well-adopted indirect method is the use of regression models utilizing a person's mass and height as inputs. The convenience of application makes this approach practical, but as BSPs are sensitive to morphology, age, and gender, the use of a regression model on persons who differ from the population that the model is developed on can result in unrepresentative estimates (19). Some of the most commonly available regression models are derived using data from cadaveric specimens of slender elderly men (20–22) and young adolescents (4). More so, height and weight as inputs to estimate mass moments of inertia and center of mass positions can be prone to error, where small changes in morphology can create large changes in these parameters, a feature that regression models are not well adapted to capture (23).

Geometrical models coupled with photographic approaches have addressed some of the aforementioned limitations. In geometrical modelling, anthropometric measurements are used to define modifiable shapes that resemble the body segments. Using mathematical principles, the BSPs can be estimated (24,25). For such an approach, the accuracy of the estimated BSPs most depends on the accuracy of the estimated geometry of the body segments, and less so, but also on, the body segment density values used in the model (26). What has deterred the widespread use of geometric modelling is the extensive experimental time necessitated for acquiring anthropometric measurements (25,27). As such, photographic approaches have been coupled with geometrical models to digitally acquire meaningful anthropometric measurements to then be used as inputs in geometric models (28,29). One such approach, the elliptical cylinder method, digitizes frontal and sagittal plane photographs to then approximate the anthropometric measures of participants and model the 3D geometry of their body using stacked elliptical cylinders. The elliptical cylinder method has been shown to be accurate to 2.0±2.2% in estimating body volume when compared to volume estimates obtained using water submersion (the gold standard in estimating volume by measuring the displacement of water) (30). However, the digitizing process can be extensive and if the use of a model to estimate the 3D geometry of the body can be mitigated, this would reduce assumptions made about the morphology (31).

3D surface scanning provides an opportunity for acquiring the 3D geometry without using a geometrical model. 3D surface scanning techniques using laser scanning (32), structured light projection (33) and time of flight cameras (34) provide the tools to 3D reconstruct objects, humans, and other animals. 3D surface scanning omits the use of predefined geometrical shapes to estimate the morphology of the body and therefore does not require the use of a 2D photographic method to make anthropometric measures. The Microsoft Kinect Version 1 (Microsoft Corporation, Redmond, USA) is a low-cost close-range camera that has shown potential for 3D volume estimation (35), for estimating participant-specific anthropometric

measurements (36), and in some preliminary work in estimating body segment parameters (37,38). Volumetric estimations using the Kinect V1 have been reported to have errors of 0.04±2.11%, suggesting greater accuracy than commonly used geometric models (38). Other 3D cameras have also shown promise in this field of research (39,40). A consumer depth camera, such as the Microsoft Kinect, presents an opportunity to develop and evaluate an inexpensive approach for estimating participant-specific BSPs while addressing some of the limitations of the aforementioned methods.

In this project, our general goal was to use 3D surface scanning to estimate participant-specific BSPs. As 3D surface scanning has shown to be a promising approach for volumetric and anthropometric measurement estimation, when used in conjunction with density values, it is certainly possible to indirectly estimate the BSPs of humans. In this project, we had three specific aims. The first aim was to develop an experimental approach for collecting participant-specific 3D scans using a readily available consumer depth camera, the Kinect Version 2 (Microsoft Corporation, Redmond, USA). The second aim was to evaluate a 3D body segmentation procedure for post-processing the 3D scans, and the third aim was to evaluate and assess the BSP estimates obtained using our proposed approach. To accomplish the first aim, we used the Kinect V2 depth camera and performed repeated 3D scans on 21 human participants. To accomplish the second aim, we used MeshLab, an open-source software (41), to segment the body into 16 body segments. To accomplish our third aim, we wrote custom software that evaluated the BSPs of the body segments acquired using our 3D scanning method. We then compared the BSPs obtained using the proposed method to estimates obtained using a camera-based geometrical modelling approach (the elliptical cylinder method (ECM) (29,42), and to estimates obtained using a regression model derived from a similar population sample.

Methods

Participants

We recruited 21 healthy adult participants for our study. The Queen's University ethics board approved the study and we obtained written consent from each participant before participation. We asked each participant to change into form-fitting shorts, a tight t-shirt, and to wear a swim cap on their heads for the 3D scanning (31). For each participant, we obtained their body mass using a medical scale, measured their stature, asked for their age, and calculated their body mass index (Table 1). We had no participant exclusion criteria.

Table 1: Participants recruited for this study

Participants	Age (Years)	Stature (m)	Mass (kg)	BMI (kg/m^2)
Males (n=10)	23.4 ± 1.7	1.8 ± 0.1	73.4 ± 4.5	22.7 ± 2.1
Females (n=11)	22.3 ± 2.4	1.7 ± 0.1	70.1 ± 8.1	23.3 ± 2.3

Experimental Setup

We used an inexpensive depth camera to perform 3D body scans. We mounted the camera, a Kinect Version 2 (Kinect V2, Microsoft Corporation, 2015) onto a generic tripod and connected it via USB 3.0 to our desktop computer. The computer was set up to operate on Windows 8.1 running an Nvidia GTX 970 graphics processing unit, a Z97 Gaming 3 intel motherboard, with 16GB of RAM. We used a 30-foot active USB 3.0 extension cord (SuperSpeed USB 3.0 Active Extension) to extend the reach of the device from the workspace computer ensuring that the camera could freely be moved around the room. We constructed a transparent platform for the participants to stand on during their 3D scans (Figure 1). This platform served to maximize the viewing of the participant's feet while minimizing the view of the floor surface. For 3D data acquisition, we used Microsoft 3D Builder (Microsoft Corporation, 2015), free software that integrates with the Kinect and saves the 3D point cloud data for viewing in a simple user interface.

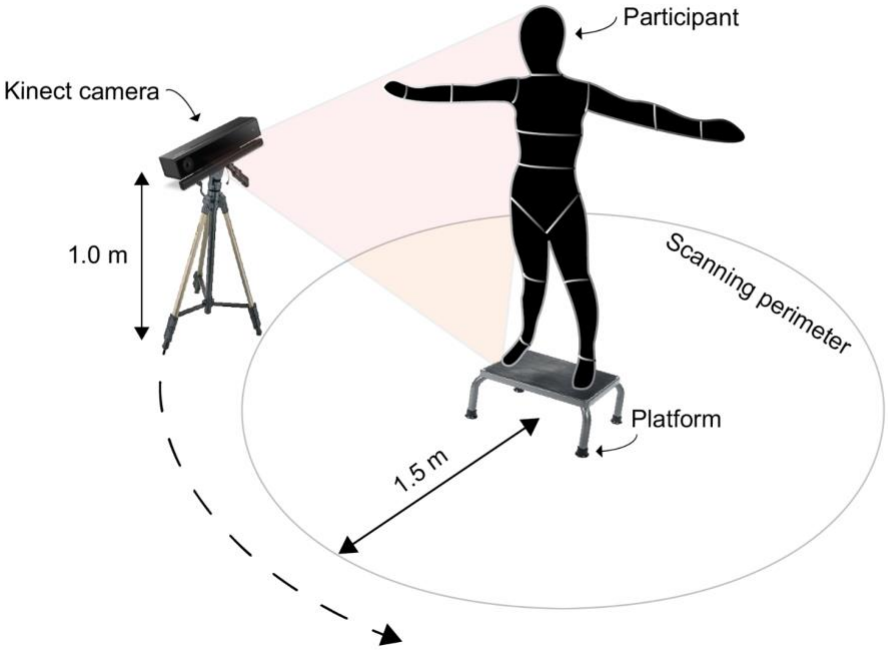

Figure 1: Experimental setup used for collecting 3D body scans. The Kinect V2 camera was manually revolved around the participant following the scanning perimeter. Participants stood with their arms abducted on a transparent platform.

Segmentation Boundaries

We placed anatomical landmarks on each participant to be used as body segmentation boundaries in post-processing. A trained operator identified landmarks in the frontal and sagittal planes and placed body markers following a set of common guidelines (see S1 File). To minimize volume artifacts, we used flat sticker markers 2cm in diameter. After we identified the anatomical landmarks, to allow for clear and repeatable segmentation boundaries, we wrapped a band of non-reflective tape around each limb such that the frontal and sagittal landmarks connected. This approach worked well in our pilot experiments and we used it here to minimize variability in limb segmentation between repeated scans by providing reproducible and clear endpoint boundaries for each body segment.

3D Scanning

Participants stood on the transparent platform while we revolved the Kinect around them to capture a 3D scan of their bodies. We asked each participant to stand with their feet separated and arms abducted at

approximately 90°. We found that this scanning posture allowed for maximal visibility underneath the arms and in between the thighs, to minimize any scanning errors resulting in skin folding when arms are together or thighs touching. Using a verbal cue "*we are now starting the 3D scan*", we vocalized to the participant the starting of the scan. At this moment the computer operator initiated the acquisition software while a second operator began to manually revolve the Kinect around the participant. The operator revolved the camera following an outlined path around the participant, holding the camera at a vertical height of 1m (**Figure 1**). After a full revolution of 360° around the participant, the operator lifted the Kinect to a higher position of ~2m by extending the legs of the trip pod rapidly and continued walking around the participant until a second revolution was complete. In pilot experiments, we found that by raising the Kinect in the second revolution a more complete view of the superior parts of the upper body segments could be captured resulting in visually more complete scans. We asked participants to remain as still as possible during the scanning process and withhold from breathing deeply to minimize any scanning artifacts (31). Once the scan was finished, we informed the participants they could relax again. We immediately reviewed the quality of the scan on the computer and considered it to meet our inclusion criteria if no visual obstructions or evident volume deformations were visible. These deformations could occur if the participants had moved or shifted their position during the scan (e.g., swaying, or moving arms). For each participant, we sought to collect 3 scans that met these inclusion criteria. Each body scan took ~30 seconds and each participant required at least 5 repetitions until 3 scans meeting our inclusion criteria were collected.

Data Analysis

We exported all 3D scans and processed them for analysis. From Microsoft 3D Builder, we exported each scan as a polygon file format (.ply) to preserve texture (i.e., colour of the pixels) for segmentation. We then imported each scan into MeshLab (64-bit v.1.3.4) (41), open-source software we used for processing and editing the 3D data. In MeshLab, we took the extraneous point cloud data, such as the floor and ceiling, and deleted it manually using the graphical user interface. Next, we aligned each scan such that the global coordinate system in MeshLab best aligned with the anatomical planes of the body (Figure 2). This approach helped us to ensure that segmentation along the frontal plane of the body was perpendicular to the plane itself allowing us to produce repeatable segmentations. Following the aforementioned alignment procedure, we segmented each scan manually into a 16-segment model using the segmentation boundaries as the guidelines (Figure 3). The body segments in the segmentation include the left and right hand, forearm, upper arm, thigh, shank, and foot as well as the head, torso, abdomen and pelvis. Finally, we saved each body segment as a Stanford triangle format (.STL) and then imported this point cloud data into MATLAB (MathWorks, 2019a) for further analysis.

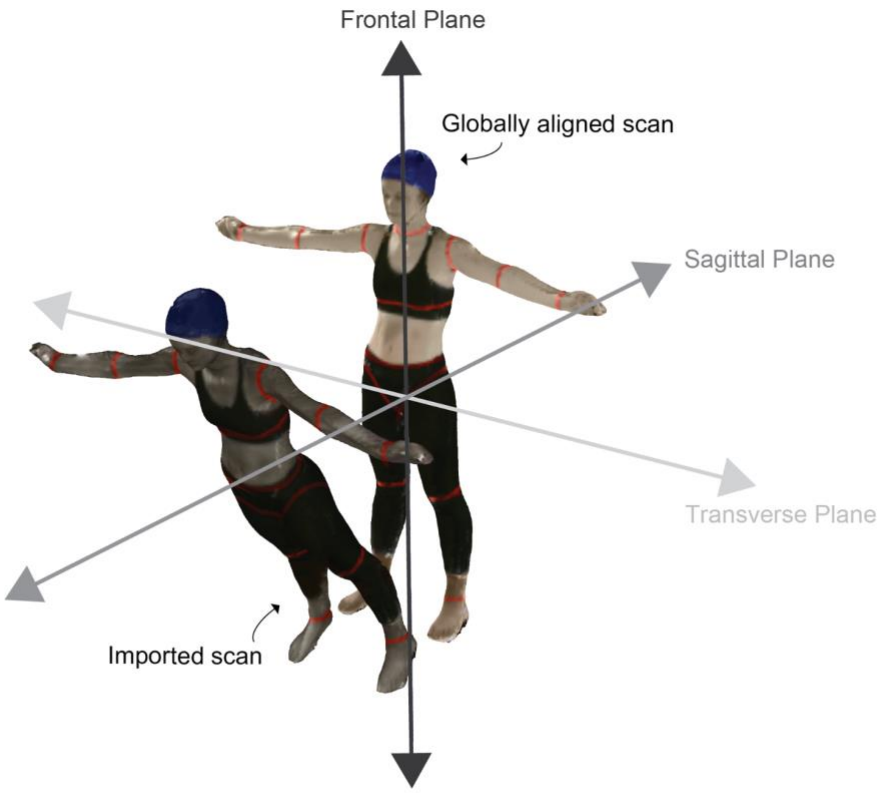

Figure 2: Imported scans were aligned such that body segment segmentation along the frontal plane was perpendicular to this plane. We aligned the imported scans to the MeshLab global coordinate system as shown.

We wrote custom-written scripts to evaluate the BSPs of each body segment. We wrote MATLAB scripts for evaluating the following outcome parameters: body segment volume, segment mass, the mass moment of inertia tensor about the center of mass of each segment, the longitudinal segment length, and the center of mass position of each segment. We calculated the total volume of each segment as the total encapsulation space of the point cloud data (43). We then determined the mass of each segment by multiplying its volume by a corresponding uniform density value (see S2 File). The density inputs we used were derived from cadavers of an older population (22) and from CT trunk estimates of a more closely related population (18). We then calculated the total body mass of each participant by adding up the mass of each of the 16 body segments. We determined the geometrical 3D center of the encapsulation space of each body segment and used this as the estimated center of mass (43). We took this approach as opposed to taking the average of all the points that describe each segment, as we found that the latter may result in small errors in the center of mass approximation (31). We calculated the segment mass moments of inertia tensor using the center of mass as the reference frame. Although we estimated the full inertial tensor, our primary interests were in

comparing principal axes of this tensor along the three orthogonal axes consisting of the anteroposterior (I_{ap}), medio-lateral (I_{ml}) and longitudinal (I_{long}) axes of each segment (for coordinate system see Figure 3). We then determined the longitudinal segmental length by projecting a vector from the center of mass position along the longitudinal axis of the segment until this line intersected a segment endpoint on each end of the segment (31). The total length was then evaluated as the distance from one endpoint to the other endpoint. We used the estimated longitudinal length of the segment to evaluate the position of the center of mass in terms of its distance from the proximal endpoint of the segment (pCOM) (see S3 File for visual definitions of longitudinal segment lengths and proximal and distal endpoints of each body segment). A high-level overview of our workflow for this experiment is shown in Figure 4.

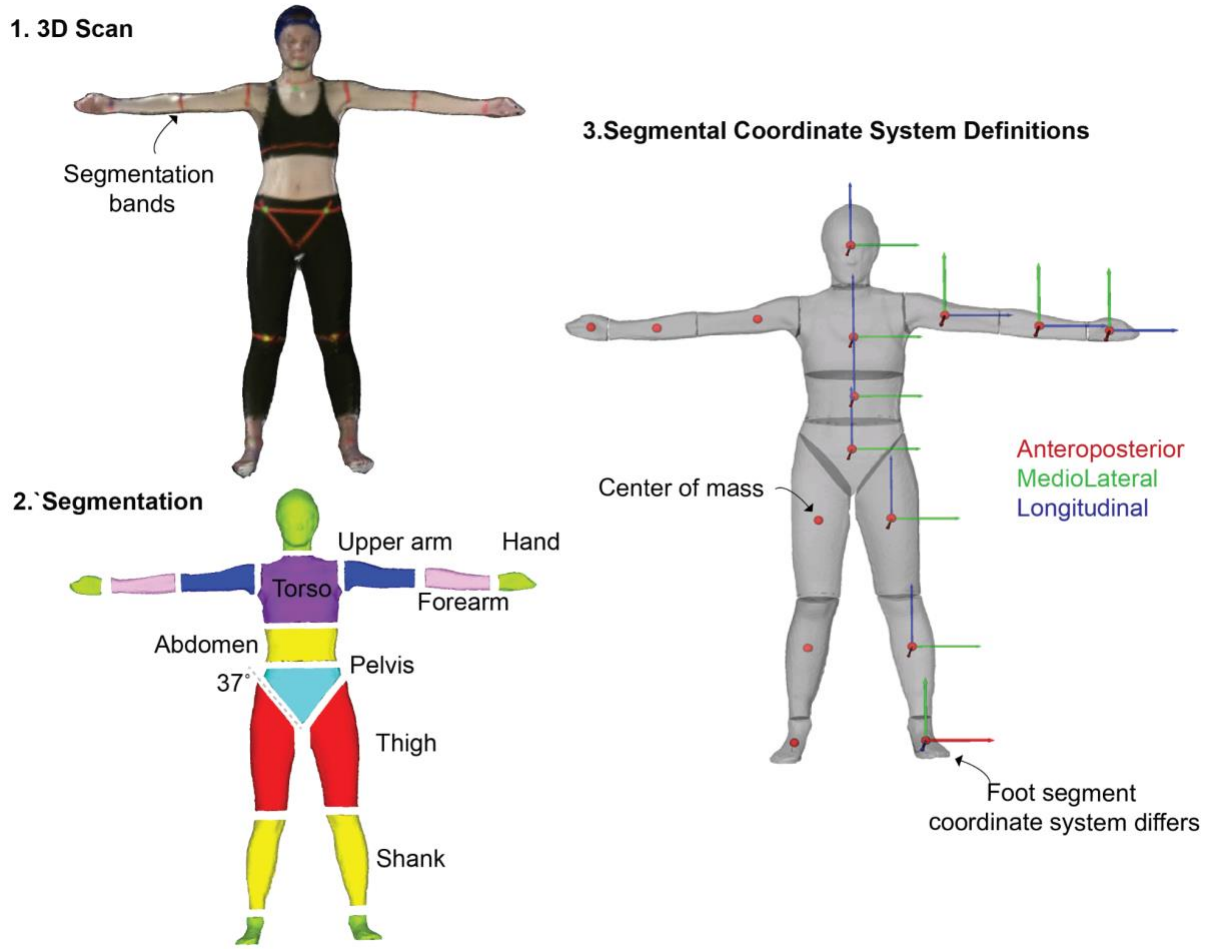

Figure 3: From 3D scan to output estimations. **1.** A representative 3D scan in MeshLab. **2.** Each 3D scan was segmented into 16 individual body segments. **3.** Segmental coordinate system definitions for each body segment showing anteroposterior (red), mediolateral (green), longitudinal (blue) axes. Here the red dot is the center of mass. The foot segment coordinate system was aligned such that the longitudinal axe was along the long length of the foot.

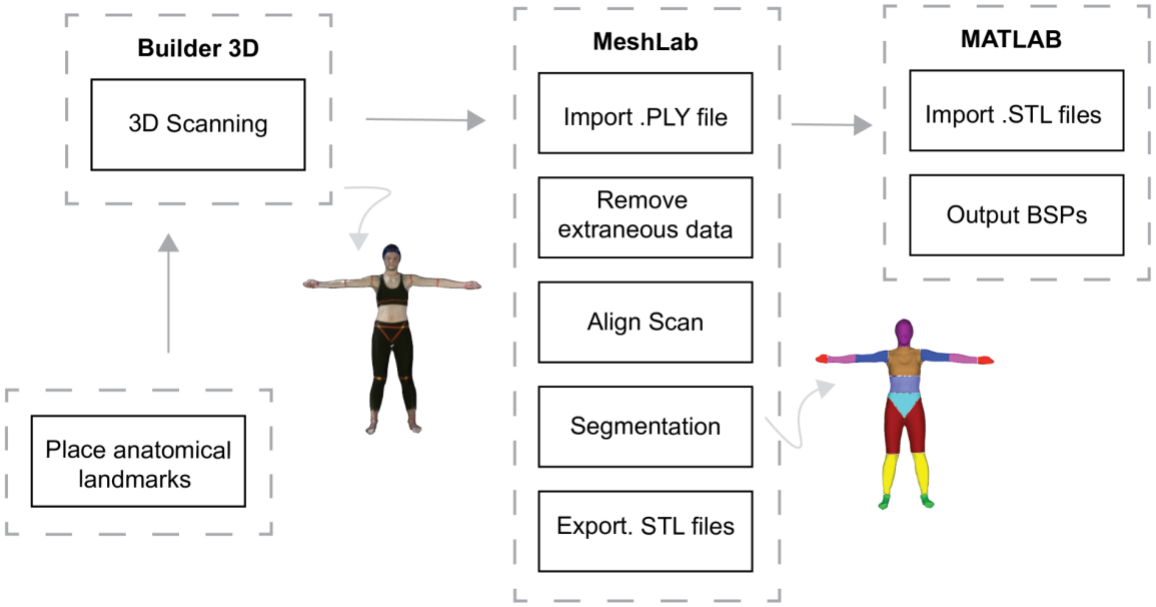

Figure 4: Overview of our workflow. After placing anatomical landmarks on the participant, we used a Microsoft Kinect V2 and Microsoft Builder 3D to collect repeated 3D body scans. We exported the acquired scans into MeshLab for removing extraneous data, globally aligning, and segmenting each scan into 16 body segments. We then wrote custom MATLAB scripts to estimate the BSPs of each body segment.

Comparison Methods

We sought to compare BSPs evaluated using the proposed method to the elliptical cylinder method (30,42). In brief, to evaluate BSPs using the elliptical cylinder method, we placed two digital cameras (Fujifilm Finepix AX 600) on tripods. Each camera was 5m from the participant at a height of 1m. One camera was oriented to capture the frontal plane and another the sagittal plane. We hung meter sticks from the ceiling to serve as a tool for image calibration in post-processing. The meter sticks were hung such that a horizontal and a vertical one were visible in each of the frontal and sagittal planes of the photographic images (see S4 File). We asked each participant to stand on an inclined platform that is commonly used in this photographic method to capture the feet (30,42). We asked participants to stand with their arms at their chest fully extended with their hands supinated and shoulders flexed (see ref (31) for more details). Once the participant was ready, we asked them to stand still while we captured the two images simultaneously, one from each camera. We imported the images into the Slicer Project (44) software that has been adapted for the elliptical cylinder method guidelines for estimating body segment parameters using the imported photographic images. A single trained operator then digitized all of the photographs using this software. Finally, we adjusted the coordinate systems for the output BSPs to best align with those evaluated using our proposed 3D scanning method for comparisons (refer to Figure 3 for specific axes definitions).

We also compared our participant-specific data to estimates obtained using a regression model. We used the regression model developed using data from a similar population pool (4). The regression model by Zatsiorsky et al. was developed using a protocol that performed medical imaging on 100 adult Caucasian males (age: 23.8±6.2 years, height: 1.74±0.06 m, mass: 73±9.1 kg, body mass index: 24) and 15 adult Caucasian females (age: 19.0±4.0 years, height: 1.74±0.03 m, mass: 61.9± 7.3 kg, body mass index: 20.5) (regression equations in S2 File). To estimate the body segment parameters of our participants, we used this regression model by using each participant's measured height and weight as inputs to the model. The similar population that these equations are derived from when compared to the participants in this study makes them a reasonable choice for use for comparison. When necessary, we adjusted the BSP axes such that the output BSPs most closely aligned with those used in our proposed method (refer to Figure 3 for axes definitions).

Scanning of a cylindrical object

To get an approximation of the relative accuracy of the device and verify our software we measured and scanned a cylindrical beam 25 times using a modified version of our 3D scanning protocol outlined above (for beam values see S5 File). We determined the mathematical approximations of the inertial parameters of this beam including total volume, longitudinal length, the proximal center of mass position, and the mass moments of inertia in the three orthogonal principal axes of the beam. We found that the 3D scanning results were similar when compared to the theoretical predictions. For example, when comparing the total volume of the beam our approach overestimated volume by +4.1%, and when comparing the longitudinal length and pCOM our approach underestimated by -0.5%. The orthogonal mass moments of inertia were well approximated using our approach with the largest difference for the longitudinal axes of the beam of +7.6%. Overall, this experiment gave us confidence that the outputs we found were within a reasonable range of what we expected to find.

Experimental Outcomes

We assessed the outcome measures here using our proposed method on males and females separately.

Total body volume

To determine the reliability in collecting 3D body scans we used each participant's total body volume obtained from each of the 3 scans which we refer to as Scan A, Scan B, and Scan C. We used a 1-way repeated-measures ANOVA to test for differences in mean total body volume between repeated scans. We also calculated the 2-way mixed-effects intraclass correlation coefficients (ICC) to provide estimates in the reliability. We considered ICC (2,1) = < 0.5 as poor, 0.50-0.75 as moderate, 0.75-0.9 as good, and >0.9 as excellent (45). Finally, we determined the coefficients of variations of body volume estimation to express

a measure of variability between repeated scans. We considered coefficients of variations of >30% as not acceptable, 20-30% as acceptable, 10-20% as good, and <10% as very good.

Total body mass

We evaluated total body mass estimates obtained using our proposed method, to those determined using the elliptical cylinder method, and to the medical scale (our gold standard mass estimate). We used a 1-way ANOVA to test for differences between the mean predicted body mass between the methods.

3D segmentation reliability

We performed the 3D body segmentation following our proposed protocol and evaluated BSPs for each body segment. The BSPs of interest were body segment masses, mass moment of inertia estimates in the anteroposterior (I_{ap}), mediolateral ($I_{frontal}$), and longitudinal (I_{long}) axes, segmental longitudinal lengths, and segmental centers of mass. To evaluate the reliability of the estimates we obtained from these measurements we calculated the coefficients of variations (CV) across the 3 separate segmentations of each body segment for each BSPs of interest. We then compared the coefficients of variations between segments across the three scans and used a 1-way repeated-measures ANOVA to test for differences between the estimated BSPs across segmentations. We compared only the right side of the body for all segments that had both a left and right side.

Body segment parameter estimates

We compared the values of the BSP estimates found using our proposed method, against the BSPs estimated obtained using the ECM approach, and to values obtained using the comparison regression analysis for each body segment (right arm, right forearm, right hand, right thigh, right shank, right foot, head torso, abdomen and pelvis). We used the mean values determined from the 3 scans when using our proposed approach and compared this against the values obtained from the ECM approach, and the regression estimates. We compared the mean segmental mass estimates, and the mass moment of inertia estimates in the anteroposterior (I_{ap}), mediolateral ($I_{frontal}$), and longitudinal (I_{long}) axes. For comparison of the estimated longitudinal segment lengths and proximal positions of the segmental centers of mass the regression equations did not provide equations for length. Therefore, we used mean values from Zatsiorsky and Seylanov for comparisons (4). We used a 1-way ANOVA to test for differences between estimates obtained using our proposed method, the ECM method, and the regression analysis for each BSP outcome.

We performed all statistical tests using the MATLAB statistical toolbox. Unless otherwise indicated, we report inter-participant means and standard deviations (SD). For the repeated-measures ANOVAs we performed a Mauchly test for sphericity. If the sphericity assumption was violated, we used epsilon

adjustments factors. In the event of a statistically significant main effect, we performed post-hoc pairwise comparisons with Bonferroni corrections (46). We set the level of significance at 0.05 for all statistical analyses.

Results

No differences in total body volume between repeated scans

The total encapsulation volume between the three repeated 3D scans did not differ significantly for both males (p=0.1194) and females (p=0.2240) (Figure 5) (for data see S6 File). The total body volume variability exhibited between repeated scans was similar for both males (SD 13.4 ± 8.9 cm^2, CV 1.8 ± 1.1 %) and females (SD 11.5 ± 5.9 cm^2, CV 1.6 ± 0.8 %) with CV<3%, corresponding to very good. We found high ICC estimates corresponding to ICC (2,1) = 0.966 for the males and ICC= (2,1) = 0.982 for the females corresponding to excellent total body volume repeatability between scans.

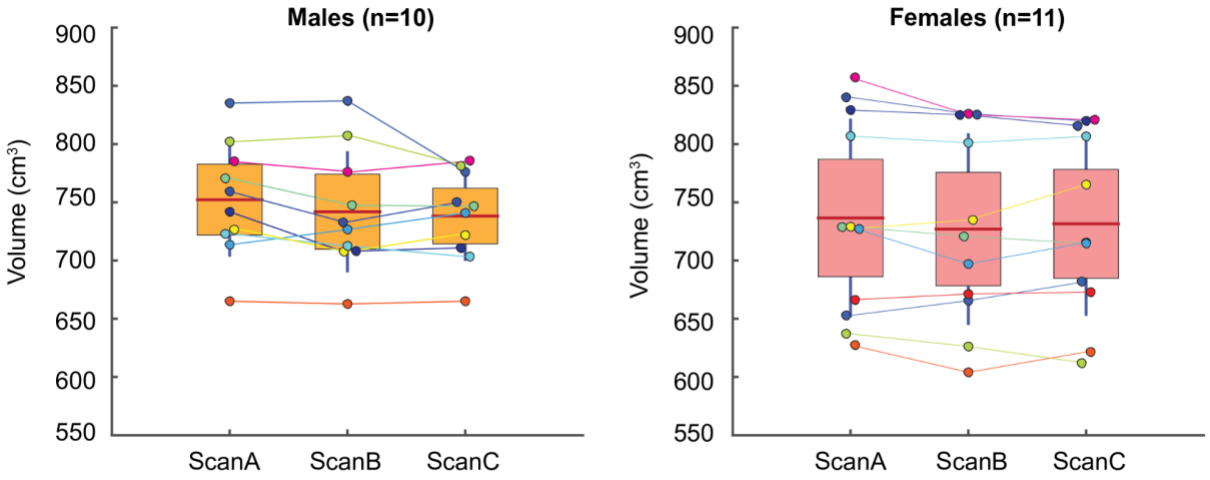

Figure 5: Total body volume estimated with our proposed 3D method for both males and females. Comparison volumes between the three scans (Scan A-C) are shown for each participant (coloured dot). The box is the 95% confidence interval around the mean (red line) and SD about the mean is shown (vertical blue line).

The 3D scanning approach provided reliable estimates of total body mass

We found that for males there were no significant differences (p=0.8529) between the average predicted total body mass estimated using the proposed method (74.5±4.5 kg), the ECM method (73.8±4.7 kg), and medical scale (73.4±4.5 kg) (Figure 6). For female participants, we found no significant differences (p=0.6339) between the average predicted total body mass estimated using the proposed method (73.2±8.0 kg), the ECM method (70.7±8.1 kg), and the medical scale (70.4±8.1 kg) (Figure 6).

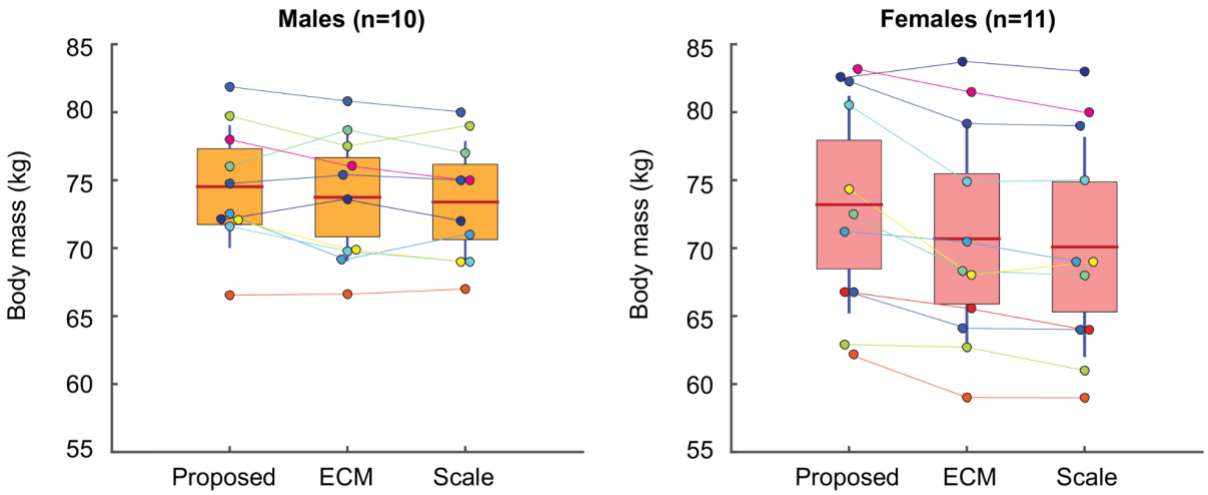

Figure 6: Body mass (kg) estimated with our proposed 3D method, the ECM method, and the medical scale for both males and females. Each participant (coloured dot). The box is the 95% confidence interval around the mean (red line) and SD about the mean is shown (vertical blue line).

The 3D segmentation approach was found to be reliable

The body segmentation of each scan (i.e., 16 body segments per scan) took ~30-40 minutes from importing to BSP estimations. The total time for post-processing decreased as we became more proficient in applying the protocol. The main fraction of this time was in the manual nature of the segmentations in MeshLab. The estimated BSPs were quite repeatable between the segmentation of the three scans, with coefficients of variations ranging largely from good (20%>CV>10%) to very good (CV<10%) criteria (Table 2). We found significant differences ($p<0.05$) between some of the repeated measures of each body segment parameter outputs (as indicated by an asterisk * in Table 2) with most differences observed in the smallest segments such as the hand and foot. These small segments also had the largest coefficients of variations for both the male and females. The larger body segments, such as the torso, had the lowest coefficients of variations. A visual representation of the segmentation for one representative male and one female participant for three repeated scans and segmentations is presented in Figure 7.

Table 2: The mean coefficients of variations (%) for repeated body segmentation of repeated 3D scans. BSPs were evaluated for each segmentation for both male and female participants. Here an asterisk (*) indicates a $p < 0.05$ for the repeated-measures comparisons.

	Male Coefficients of variation (%)						Female Coefficients of variation (%)					
Segment	**Volume**	**I_{ap}**	**I_{ml}**	**I_{long}**	**Length**	**pCOM**	**Volume**	**I_{ap}**	**I_{ml}**	**I_{long}**	**Length**	**pCOM**
Head	3.0	7.0	6.3*	4.0	2.7*	0.8	4.0	8.7	7.4	5.8	2.9	2.0
Torso	2.9	5.1	6.2	4.0	3.8	1.7	3.6	6.8	7.4	4.1	4.1	1.6
Ab	2.9	4.9	6.1	4.0	2.8	0.8	2.8	4.0	5.4*	3.2	2.9*	2.0
Pelvis	4.4	8.2	6.6	6.0	4.7*	2.4	7.7	14.3	11.3	10.5	5.9	3.0
Thigh	4.6	8.1*	8.1*	8.0	2.4*	1.2	3.3	7.1	7.5	5.2	2.7	1.4
Shank	5.7	6.9	7.0	11.0	1.3	0.8*	3.5	5.1	5.3	6.1	1.1	1.4
Foot	13.2	19.4	19.1	25.0	5.1	5.1*	11.0*	16.1*	15.2*	19.3	3.9	4.7
Arm	9.5*	19.8	20.4	18.0	4.3*	2.4	7.4	11.7	12.5	14.4	3.0	3.5
Forearm	7.1	12.8	12.9	10.0	3.3	1.8	13.3	19.9	21.1	19.2	3.7	2.6
Hand	16.6*	30*	30.7*	23.7*	8.9*	4.9	20.2*	30.3*	30.9*	29.8*	9.2	3.9

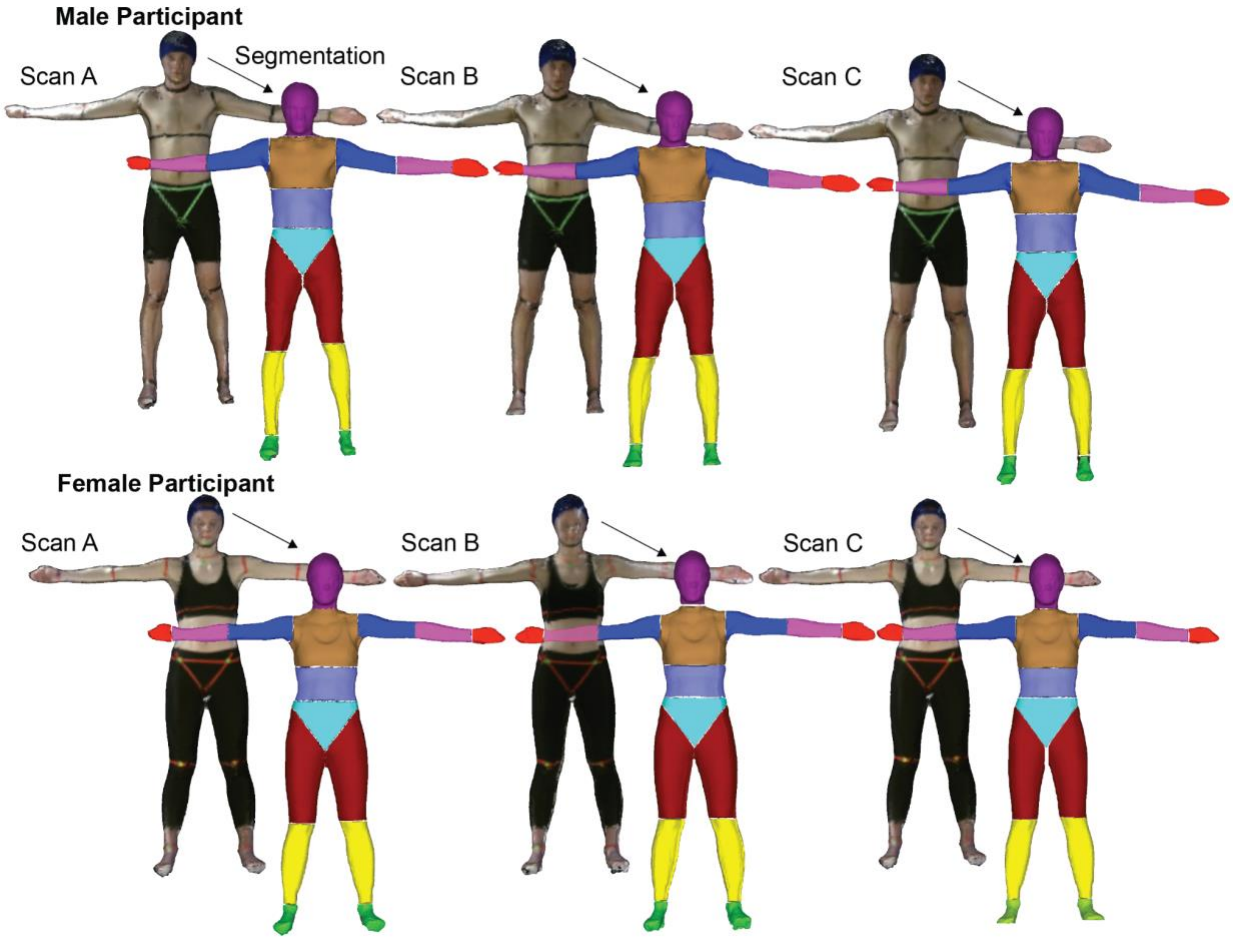

Figure 7: Three different scans (Scan A, Scan B, Scan C) and three individual body segmentations from a representative male and female participant are shown. The colouring used for the segmented scan is meant to show clear segmentation borders between adjacent body segments.

Found BSPs well-matched the comparison methods

We found that the proposed method reliably estimated participant-specific BSPs providing estimates that were comparable to those determined using the ECM and the regression modelling approaches. The body segment mass estimates (Table 3), mass moments of inertia estimates in the anteroposterior (I_{apl}), mediolateral ($I_{frontal}$), and longitudinal (I_{lg}) principal axes from each segments center of mass reference frame (Table 4), longitudinal segment lengths (Table 5), and the proximal centers of mass (Table 6) are shown.

Table 3: Body segment mass estimates (mean±SD in kg) obtained using the proposed method, the ECM approach, and regression modelling for both male and female participants. Significant differences ($p<0.05$) found in post-hoc analysis are reported as symbols. Where '○' indicates a significant between the proposed and the ECM method, '●' indicates a significant difference between the proposed and the regression modelling, and '∆' indicates a significant difference between ECM and regression modelling.

	Male Segment Mass (kg)									**Female Segment Mass (kg)**								
Segment	**Proposed**			**ECM**				**Regression**			**Proposed**			**ECM**				**Regression**	
Head	5.6	±	0.4	●	5.7	±	0.3	∆	5.1	±	0.1	5.3	±	0.4		5.4	±	0.6	∆	4.9	±	0.1
Up-Trunk	11.5	±	1.0	○	10.1	±	0.8	∆	11.4	±	0.8	12.0	±	2.0		10.4	±	2.0		10.5	±	1.9
Abdomen	11.0	±	1.6		10.5	±	1.7		11.7	±	1.0	7.0	±	1.2	●	6.4	±	0.9	∆	9.1	±	0.7
Pelvis	9.2	±	0.8	●	8.9	±	0.6		8.4	±	0.6	8.9	±	1.4		8.5	±	1.6		8.5	±	1.2
Thigh	10.4	±	0.8		10.4	±	1.0		10.5	±	0.7	12.0	±	1.4		11.7	±	1.5		10.7	±	1.3
Shank	3.5	±	0.4		3.6	±	0.5		3.2	±	0.2	3.9	±	0.5	●	3.8	±	0.5	∆	2.9	±	0.2
Foot	1.1	±	0.2		1.1	±	0.2		1.0	±	0.1	1.1	±	0.2	●	1.0	±	0.1	∆	1.5	±	0.1
Arm	2.1	±	0.2		2.3	±	0.3	∆	2.0	±	0.1	1.9	±	0.2		2.0	±	0.3	∆	1.7	±	0.1
Forearm	1.1	±	0.1		1.2	±	0.2		1.2	±	0.1	0.9	±	0.2		1.0	±	0.1		1.0	±	0.1
Hand	0.5	±	0.1	○	0.7	±	0.1	∆	0.5	±	0.0	0.4	±	0.1	○	0.5	±	0.1	∆	0.4	±	0.0

Table 4: Moment of inertia estimates (mean±SD in kg cm^2) obtained using the proposed method, the ECM approach, and regression modelling for both male and female participants. Significant differences ($p<0.05$) found in post-hoc analysis are reported as symbols. Where '○' indicates a significant between the proposed and the ECM method, '●' indicates a significant between the proposed and the regression modelling, and '△' indicates a significant between ECM and regression modelling.

	Male I_{ap} (kg cm^2)				**Female I_{ap} (kg cm^2)**			
Segment	**Proposed**	**ECM**	**Regression**		**Proposed**	**ECM**	**Regression**	
Head	289 ± 36	○	248 ± 35	280 ± 12	261 ± 38	○|●	197 ± 34	226 ± 1
Up-Trunk	1839 ± 258	○	1237 ± 175	△ 1708 ± 158	1874 ± 517	○	1355 ± 456	1434 ± 376
Abdomen	1037 ± 244		962 ± 276	△ 1234 ± 174	503 ± 134	●	438 ± 96	△ 732 ± 68
Pelvis	635 ± 100		650 ± 104	700 ± 82	620 ± 149		641 ± 262	709 ± 144
Thigh	1682 ± 183	●	1866 ± 288	2104 ± 209	2028 ± 431		2086 ± 459	2082 ± 477
Shank	394 ± 67		454 ± 84	420 ± 52	392 ± 90		457 ± 116	354 ± 73
Foot	48 ± 14		49 ± 9	47 ± 5	43 ± 17		41 ± 11	39 ± 8
Arm	156 ± 35	○	197 ± 36	△ 135 ± 13	138 ± 32		146 ± 32	126 ± 15
Forearm	55 ± 12	○|●	70 ± 12	67 ± 5	43 ± 15		49 ± 12	54 ± 12
Hand	8 ± 5	○|●	17 ± 4	14 ± 1	6 ± 2	○|●	11 ± 3	9 ± 1
	I_{ml} (kg cm^2)				**I_{ml} (kg cm^2)**			
Head	331 ± 4	○|●	278 ± 39	303 ± 14	323 ± 5	○|●	255 ± 46	259 ± 11
Up-Trunk	1057 ± 170	○|●	825 ± 115	684 ± 80	1319 ± 385	○|●	977 ± 318	△ 648 ± 193
Abdomen	754 ± 194		683 ± 187	790 ± 116	335 ± 108	●	290 ± 74	△ 540 ± 65
Pelvis	688 ± 112	●	680 ± 107	△ 548 ± 63	645 ± 178		647 ± 180	516 ± 101
Thigh	1756 ± 189	●	1959 ± 291	2107 ± 213	2126 ± 449		2213 ± 467	2077 ± 449
Shank	397 ± 68		463 ± 87	406 ± 53	392 ± 93		430 ± 170	350 ± 71
Foot	45 ± 11		48 ± 9	43 ± 5	40 ± 15		38 ± 15	33 ± 6
Arm	148 ± 37	○	205 ± 37	△ 121 ± 12	129 ± 28		132 ± 63	100 ± 23
Forearm	55 ± 13	○	68 ± 11	62 ± 5	42 ± 15		44 ± 16	53 ± 12
Hand	8 ± 5	○	14 ± 3	△ 9 ± 1	5 ± 2	○	9 ± 3	△ 6 ± 1

	I_{lg} (kg cm^2)										I_{lg} (kg cm^2)									
Head	200	±	26		186	±	26		202	±	8	190	±	23		199	±	60		176	±	21
Up-Trunk	1632	±	255	○	1040	±	152	∆	1418	±	156	1563	±	477	○	1015	±	348		1205	±	297
Abdomen	1018	±	237		959	±	253		1121	±	198	616	±	198		553	±	143	∆	736	±	79
Pelvis	767	±	117	○ ●	631	±	66		606	±	70	753	±	207		575	±	185		739	±	184
Thigh	413	±	60		403	±	61		408	±	49	533	±	110	●	509	±	118	∆	346	±	64
Shank	54	±	11	●	56	±	13		67	±	6	72	±	15		97	±	111		52	±	6
Foot	14	±	5	○| ●	8	±	2	∆	1	±	1	12	±	4	●	10	±	8	∆	37	±	2
Arm	32	±	7	●	27	±	6	∆	40	±	3	30	±	8		43	±	44		41	±	13
Forearm	8	±	3	●	10	±	3		12	±	1	6	±	2		10	±	12		8	±	1
Hand	3	±	2	○| ●	6	±	1		6	±	1	2	±	1	○	4	±	2		3	±	1

Table 5: Longitudinal length estimates (mean±SD in cm) obtained using the proposed method and the ECM approach for both male and female participants. Significant differences ($p<0.05$) found in post-hoc analysis are reported as symbols. Where '○' indicates a significant difference between the proposed and the ECM method. Average values of longitudinal length estimates published by (Paolo de Leva, 1996) (as shown in Table A2.11 and Figure A.3 in (4) are shown from reference. (Here # indicates no data provided).

	Male Length (cm)			Female Length (cm)		
Segment	**Proposed**	**ECM**	**Avg. Value**	**Proposed**	**ECM**	**Avg. Value**
Head	25.6 ± 0.8 ○	28.9 ± 0.9	24.3 ± #	26.0 ± 1.3 ○	28.4 ± 1.4	24.6 ± #
Up-Trunk	24.9 ± 1.5 ○	23.8 ± 1.6	24.2 ± #	28.3 ± 2.9	27.3 ± 2.7	22.8 ± #
Abdomen	20.2 ± 1.9	20.5 ± 2.1	21.6 ± #	13.6 ± 1.0	15.9 ± 4.5	20.5 ± #
Pelvis	23.4 ± 1.2 ○	18.8 ± 1.7	25.2 ± #	22.6 ± 1.4 ○	21.4 ± 2.3	* ± #
Thigh	46.3 ± 1.5	47.6 ± 3.4	42.2 ± #	47.2 ± 2.4 ○	42.6 ± 3.6	36.9 ± #
Shank	40.2 ± 1.4 ○	41.5 ± 2.0	44.0 ± #	38.5 ± 2.6 ○	40.4 ± 3.0	43.9 ± #
Foot	24.5 ± 1.0 ○	22.3 ± 0.4	25.8 ± #	23.7 ± 1.5 ○	21.6 ± 1.3	22.8 ± #
Arm	28.1 ± 2.0	28.2 ± 1.8	28.2 ± #	29.0 ± 2.3 ○	26.7 ± 2.6	27.5 ± #
Forearm	25.7 ± 0.9 ○	27.4 ± 1.2	26.9 ± #	24.8 ± 2.5	26.1 ± 2.0	26.4 ± #
Hand	15.3 ± 1.9 ○	20.0 ± 1.3	18.8 ± #	14.2 ± 1.7 ○	19.0 ± 1.1	17.0 ± #

Table 6: Center of mass position from the proximal endpoints (pCOM) (mean±SD in %) estimated using the proposed method and the ECM approach for both male and female participants. Significant differences ($p<0.05$) found in post-hoc analysis are reported as symbols. Where '○' indicates a significant difference between the proposed and the ECM method. The regression equations provided by Zatsiorsky and Seluyanov provide pCOM in mm along the longitudinal axis without providing the longitudinal length. As such we report the average values from the study adjusted to best match our definitions of pCOM (based on Table 4.4 and Table A2.5 in (4))

	Male pCOM (%)			Female pCOM(%)		
Segment	**Proposed**	**ECM**	**Mean Value**	**Proposed**	**ECM**	**Mean Value**
Head	49.6 ± 0.9 ○	46.5 ± 1.2	50.0 ± 2.2	48.3 ± 1.3 ○	45.4 ± 1.8	48.4 ± #
Up-Trunk	54.8 ± 0.9 ○	58.8 ± 2.7	50.7 ± 2.2	57.2 ± 1.1	56.6 ± 1.9	50.5 ± #
Abdomen	48.6 ± 1.0 ○	51.2 ± 1.5	45.0 ± 2.1	50.0 ± 1.6	48.6 ± 9.2	45.1 ± #
Pelvis	36.5 ± 1.1 ○	52.3 ± 5.0	35.4 ± 3.0	36.6 ± 1.3 ○	45.8 ± 6.2	34.8 ± #
Thigh	44.0 ± 1.0	44.7 ± 3.5	41.0 ± 1.9	44.7 ± 1.3 ○	38.2 ± 4.8	46.1 ± #
Shank	40.6 ± 1.1	40.0 ± 1.9	44.0 ± 2.8	40.9 ± 0.8	41.2 ± 1.3	40.3 ± #
Foot	45.1 ± 1.9 ○	39.1 ± 2.5	44.2 ± 3.7	44.6 ± 2.3	38.2 ± 2.1	40.1 ± #
Arm	41.9 ± 1.4	48.2 ± 29.8	42.3 ± 4.2	40.9 ± 1.0	41.4 ± 3.5	44.0 ± #
Forearm	41.2 ± 1.6 ○	42.9 ± 1.6	42.7 ± 3.3	42.7 ± 1.5	43.9 ± 2.5	42.6 ± #
Hand	40.7 ± 1.2	40.7 ± 2.5	36.9 ± 4.9	42.9 ± 2.7	40.6 ± 4.1	35.0 ± #

Discussion

We evaluated an inexpensive 3D surface scanning approach for estimating participant-specific BSPs. We used a readily available consumer depth camera, the Kinect V2 to collect repeated 3D body scans of 21 healthy participants. Our approach was straightforward to implement, low cost and produced reliable total volume estimates between repeated 3D body scans. We found that there were no differences between the total volume when comparing repeated scans for both male and female participants with high ICC (2,1) $\geq$ 0.95 values. Our proposed 3D segmentation protocol and post-processing of 3D scans worked well. Using open-source software MeshLab and without much operator training, we were able to segment each scan into 16 individual body segments. From importing the 3D scan to outputted BSPs it took ~30-40 min per scan with the amount of time decreasing as we became proficient in the protocol. Finally, we estimated the participant-specific BSPs using the segmented scans and compared these BSP results to those found using the two comparison methods. We found that our proposed method compared well with the other two methods. We found that the smallest body segments (e.g., foot and hand) had the largest differences between comparison methods.

This study has several limitations. One limitation is the manual nature of segmenting the 3D scans and the reliance here on the placed landmarks. The landmarks had a high contrast between the participant and their skin, providing us with segmentation boundaries. Poor visibility of these landmarks and the tape used to define the segmentation boundaries create an opportunity for segmentation boundary errors. Although we generally found good coefficients of variations between repeated segmentations, when the visibility of the segmentation boundary was poor, we had to rely on our best judgment to make the segmentation. Developing a more automatic segmentation process would reduce the time requirements in post-processing and may remove the need for the lengthy process of physically placing skin markers and then using them for segmentation (47). A second limitation is the scan duration. Each 3D scan took ~30 seconds where the participant was required to stand still. This is enough time for body sway and the lungs movement during breathing to perturb the measured volume. To minimize this effect, we asked participants to remain still and refrain from deeper breathing, but such a long-time requirement can be problematic when working with populations that may have difficulty in standing still (e.g., children or persons with disabilities). Although our proposed method did work well, integrating multiple cameras could reduce scan time requirements and may indeed improve our methods in the future (19,42,48).

The depth camera has certain limitations that need to also be considered. Firstly, when we encircled the Kinect V2 around our participants, their arms came significantly closer to the camera than any other body part. This may have contributed to some of the poor texture and lack of finer detail observed in some of the segments (Figure 8). The optimal accuracy of the Kinect V2 depth perception is in the 0.5-2m range away from the participant, where the camera has depth perception errors of less than 2mm (49). Scanning distances of less than 0.5m away, which would be the case for participants who had an arm's length of more than 0.5m, would enter this suboptimal and likely more error-prone field of view (49). 3D scanning of curved, concave, and sharp edges is also a known limitation with 3D scanning technologies. Error-prone surfaces may be smoothed out when perceiving depth (34,49). To minimize this in our protocol, we asked participants to keep their hands open during scanning as a means of preventing concavity when the hands are supinated. However, visual occlusion of other concave surfaces is still evident, such as on the face (Figure 8). For females with larger breasts, the gap between the breasts may have been overestimated, especially since most participants wore a shirt. As our approach estimated upper trunk masses about ~2kg higher for females (Table 5) when compared to the ECM approach, these overestimations may be partially due to sensor limitations for convex regions and gaps. Lastly, the depth perception of the device is a function of operating time where after ~40 minutes of operating and warming up, the depth perception reaches a steady-state value (50). Although depth differences between using the device right away and using the device after it has been warmed up are suggested to be small (~0.003m^2), the effects of this were not included in our study but may be important to consider when using this device.

Figure 8: Top view of full-body, head and hand scans. **1.** An example showing lack of texture in the scan on the upper arm regions. **2.** Varied degree of detail in the head region with concave surfaces appears as filled in. Further to the right head suggests minor sway, as facial features are distorted more so than the head to the left. Hands showing varied degree of detail.

Our findings suggest that 3D surface scanning is a viable candidate for body segment parameters estimation from participants of interest. 3D scanning, in general, provides an exciting opportunity for estimating a wide range of body segment parameters without the need for geometric models or many predefined assumptions about the body, the age, or ethnic background of a person. Indeed, we did assume uniform densities for our evaluation of body segments. However, different density values or non-uniform density functions could be implemented into our workflow, speaking to the flexibility of a surface scanning approach with programmatic and easily modifiable inputs. Although we did not evaluate it, a non-uniform density assumption may have little effect on the estimated outputs (51). The most evident discrepancies between the outputs from our proposed 3D scanning method compared to the elliptical cylinder method were in the longitudinal lengths and the proximal center of mass estimates. But it is important to understand that the elliptical cylinder method estimates are also estimates provide only an approximate value for the BSPs. As BSPs are difficult to precisely estimate, especially for inner segments such as the trunk, pelvis, and thighs, the differences we see may be partially attributed to differences between the exact segmentation boundaries of each segment, the variation in the 2D vs 3D approaches, and the elliptical shape assumptions that the ECM approach is based on (30,42).

Here we evaluated a low-cost, easy-to-implement 3D scanning method that can be widely available for implementation by others. As we have shown, the system can well estimate participant-specific BSPs providing consistent and reliable outputs for a range of body segment parameters. The body segmentation method we developed and used can also be adapted to be used with 3D scans acquired using different cameras and different approaches. Although there is no limitation on how the 3D scan is acquired and used using our methods, future work could focus on the evaluation of other devices for acquiring 3D scans. A 3D scanning approach enables measurements and estimated BSPs to be specific to the person of interest without reliance on prior assumptions on the geometry of their bodies.

Supporting Information

S1 File. Anatomical landmarking guidelines.

S2 File. Density values and regression equations.

S3 File. Longitudinal length and center of mass definitions.

S4 File. Elliptical cylinder method setup.

S5 File. Scanning of cylindrical tube.

S6 File. Participant volumes for repeated scans

Acknowledgements

We thank all of our participants who volunteered their time for our study and Professor Michael Rainbow for guidance.

Funding

Funding for this study was provided by NSERC Canada Discovery Grant A6858

Author Contributions

Pawel Kudzia conceived and designed the experiments, performed the experiments, analyzed the data, wrote the paper, prepared figures and tables and reviewed all drafts of the paper.

Erika Jackson assisted with the experiments and reviewed all drafts of the paper.

Genevieve Dumas conceived and designed the experiments, provided guidance throughout the project, acquired funding and reviewed all drafts of the paper.

References

1. Narang YS, Murthy Arelekatti VN, Winter AG 5th. The Effects of the Inertial Properties of Above-Knee Prostheses on Optimal Stiffness, Damping, and Engagement Parameters of Passive Prosthetic Knees. Journal of Biomechanics Eng [Internet]. 2016 Dec 1;138(12). Available from: http://dx.doi.org/10.1115/1.4034168

2. Van Soest AJ (knoek), Peper C (lieke) E, Selles R (ruud) W. Mass Perturbation of a Body Segment: I. Effects on Segment Dynamics. J Mot Behav. 2004 Nov 1;36(4):419–24.

3. Das B, Sengupta AK. Industrial workstation design: a systematic ergonomics approach. Appl Ergon. 1996 Jun;27(3):157–63.

4. Zatsiorsky VM, Zaciorskij VM. Kinetics of Human Motion. Human Kinetics; 2002. 653 p.

5. Arena SL, McLaughlin K, Nguyen A-D, Smoliga JM, Ford KR. A Comparison of Body Segment Inertial Parameter Estimation Methods and Joint Moment and Power Calculations During a Drop Vertical Jump in Collegiate Female Soccer Players. Journal of Applied Biomechanics. 2017 Feb 1;33(1):76–9.

6. Jackson E. Body Segment Inertial Parameters of Toddlers. Queen's University ; 2017. Available from: https://qspace.library.queensu.ca/handle/1974/15927

7. Chambers AJ, Sukits AL, McCrory JL, Cham R. The effect of obesity and gender on body segment parameters in older adults. Clinical Biomechanics. 2010 Feb;25(2):131–6.

8. Andrews JG, Mish SP. Methods for investigating the sensitivity of joint resultants to body segment parameter variations. Journal of Biomechanics. 1996 May;29(5):651–4.

9. Silva MPT, Ambrósio JAC. Sensitivity of the results produced by the inverse dynamic analysis of a human stride to perturbed input data. Gait Posture. 2004 Feb;19(1):35–49.

10. Pataky TC, Zatsiorsky VM, Challis JH. A simple method to determine body segment masses in vivo: reliability, accuracy and sensitivity analysis. Clinical Biomechanics. 2003 May;18(4):364–8.

11. Pearsall DJ, Costigan PA. The effect of segment parameter error on gait analysis results. Gait Posture. 1999 Jul;9(3):173–83.

12. Rao G, Amarantini D, Berton E, Favier D. Influence of body segments' parameters estimation models on inverse dynamics solutions during gait. Journal of Biomechanics. 2006;39(8):1531–6.

13. Kwon Y-H. Effects of the Method of Body Segment Parameter Estimation on Airborne Angular Momentum. J Appl Biomech. 1996 Nov 1;12(4):413–30.

14. Sunaga Y, Kanemura N, Anan M, Takahashi M, Shinkoda K. Estimation of inertial parameters of the lower trunk in pregnant Japanese women: A longitudinal comparative study and application to motion analysis. Appl Ergon. 2016 Jul; 55:173–82.

15. Laschowski B, McPhee J. Body segment parameters of Paralympic athletes from dual-energy X-ray absorptiometry. Sports Eng. 2016;19(3):155–62.

16. Cheng CK, Chen HH, Chen CS, Chen CL, Chen CY. Segment inertial properties of Chinese adults

598 determined from magnetic resonance imaging. Clinical Biomechanics. 2000 Oct;15(8):559–66.

599 17. Ho W-H, Shiang T-Y, Lee C-C, Cheng S-Y. Body segment parameters of young Chinese men
600 determined with magnetic resonance imaging. Med Sci Sports Exercise. 2013 Sep;45(9):1759–66.

601 18. Pearsall DJ, Reid JG, Livingston LA. Segmental inertial parameters of the human trunk as
602 determined from computed tomography. Ann Biomed Eng. 1996 Mar;24(2):198–210.

603 19. Peyer KE, Morris M, Sellers WI. Subject-specific body segment parameter estimation using 3D
604 photogrammetry with multiple cameras. PeerJ. 2015 Mar 10;3:e831.

605 20. Dempster WT. Space requirements of the seated operator, geometrical, kinematic, and mechanical
606 aspects of the body with special reference to the limbs [Internet]. Michigan State Univ East Lansing;
607 1955. Available from: https://apps.dtic.mil/dtic/tr/fulltext/u2/087892.pdf

608 21. Clauser CE, McConville JT, Young JW. Weight, volume, and center of mass of segments of the
609 human body [Internet]. Antioch Coll Yellow Springs OH; 1969. Available from:
610 https://apps.dtic.mil/dtic/tr/fulltext/u2/710622.pdf

611 22. Chandler RF, Clauser CE, McConville JT, Reynolds HM, Young JW. Investigation of inertial
612 properties of the human body [Internet]. Air Force Aerospace Medical Research Lab Wright-
613 Patterson AFB OH; 1975. Available from: https://apps.dtic.mil/sti/citations/ADA016485

614 23. Damavandi M, Barbier F, Leboucher J, Farahpour N, Allard P. Effect of the calculation methods on
615 body moment of inertia estimations in individuals of different morphology. Med Eng. Phys. 2009
616 Sep;31(7):880–6.

617 24. Durkin JL, Dowling JJ. Body segment parameter estimation of the human lower leg using an
618 elliptical model with validation from DEXA. Ann Biomed Eng. 2006 Sep;34(9):1483–93.

619 25. Hatze H. A mathematical model for the computational determination of parameter values of
620 anthropomorphic segments. Journal of Biomechanics. 1980;13(10):833–43.

621 26. Wicke J, Dumas GA. A new geometric-based model to accurately estimate arm and leg inertial
622 estimates. Journal of Biomechanics. 2014 Jun 3;47(8):1869–75.

623 27. Dembia C, Moore JK, Hubbard M. An object-oriented implementation of the Yeadon human inertia
624 model. F1000Res. 2014 Sep 17;3(223):223.

625 28. Deffeyes J, Sanders R. Elliptical zone body segment modelling software: digitising, modelling and
626 body segment parameter calculation. In: ISBS-Conference Proceedings Archive [Internet].
627 ojs.ub.uni-konstanz.de; 2005. Available from: https://ojs.ub.uni-konstanz.de/cpa/article/view/1174

628 29. Chiu C-Y, Pease DL, Fawkner S, Sanders RH. Validation of Body Volume Acquisition by Using
629 Elliptical Zone Method. Int J Sports Med. 2016 Dec;37(14):1117–23.

630 30. Wicke J, Lopers B. Validation of the volume function within Jensen's (1978) elliptical cylinder
631 model. Journal of Applied Biomechanics. 2003;19(1):3–12.

632 31. Kudzia P. Estimating Body Segment Inertial Parameters of the Human Body Using a Microsoft
633 Kinect [Internet]. Queen's University ; 2015. Available from:
634 https://qspace.library.queensu.ca/handle/1974/13813

32. Pandis P, Bull AM. A low-cost three-dimensional laser surface scanning approach for defining body segment parameters. Proc Inst Mech Eng. H. 2017 Nov;231(11):1064–8.

33. Stančić I, Musić J, Zanchi V. Improved structured light 3D scanner with application to anthropometric parameter estimation [Internet]. Vol. 46, Measurement. 2013. p. 716–26. Available from: http://dx.doi.org/10.1016/j.measurement.2012.09.010

34. Sarbolandi H, Lefloch D, Kolb A. Kinect range sensing: Structured-light versus Time-of-Flight Kinect. Computer Vision Image Understanding. 2015 Oct 1; 139:1–20.

35. Buffa R, Mereu E, Lussu P, Succa V, Pisanu T, Buffa F, et al. A new, effective and low-cost three-dimensional approach for the estimation of upper-limb volume. Sensors. 2015 May 26;15(6):12342–57.

36. Espitia-Contreras A, Sanchez-Caiman P. Development of a Kinect-based anthropometric measurement application. 2014 IEEE Virtual [Internet]. 2014

37. Kongsro J. Estimation of pig weight using a Microsoft Kinect prototype imaging system. Computer Electron Agric. 2014 Nov 1; 109:32–5.

38. Clarkson S, Choppin S, Hart J, Heller B, Wheat J. Calculating body segment inertia parameters from a single rapid scan using the Microsoft Kinect. In: Proceedings of the 3rd international conference on 3D body scanning technologies. seanclarkson.com; 2012. p. 153–63.

39. Smith SHL, Bull AMJ. Rapid calculation of bespoke body segment parameters using 3D infra-red scanning. Med Eng. Phys. 2018 Dec; 62:36–45.

40. Chiu C-Y, Pease DL, Sanders RH. Effect of different standing poses on whole body volume acquisition by three-dimensional photonic scanning. IET Science, Measurement & Technology. 2016 Sep 1;10(6):553–6.

41. Cignoni P, Callieri M, Corsini M, Dellepiane M, Ganovelli F, Ranzuglia G. MeshLab: an Open-Source Mesh Processing Tool [Internet]. Eurographics Italian Chapter Conference. The Eurographics Association; 2008 [cited 2020 Nov 20].

42. Jensen RK. Estimation of the biomechanical properties of three body types using a photogrammetric method. Journal of Biomechanics. 1978;11(8-9):349–58.

43. Eberly D, Lancaster J, Alyassin A. On gray scale image measurements: II. Surface area and volume. CVGIP: Graphical Models and Image Processing. 1991 Nov 1;53(6):550–62.

44. McIlwain J. Slicer [Computer Software]. Author, Sudbury, Ont. 1998;

45. Koo TK, Li MY. A Guideline of Selecting and Reporting Intraclass Correlation Coefficients for Reliability Research. J Chiropr Med. 2016 Jun;15(2):155–63.

46. Sedgwick P. Multiple significance tests: the Bonferroni correction. BMJ [Internet]. 2012 Jan 25 [cited 2021 May 12];344. Available from: https://www.bmj.com/content/344/bmj.e509

47. Ahmad O, Debanne P, Parent S, Labelle H, Cheriet F. Torso shape extraction from 3D body scanning data using automatic segmentation tool. In: Proceedings of 3DBODYTECH 2017 - 8th International Conference and Exhibition on 3D Body Scanning and Processing Technologies, Montreal QC, Canada, 11-12 Oct 2017 [Internet]. Ascona, Switzerland: Hometrica Consulting - Dr.

Nicola D'Apuzzo; 2017. Available from:
https://www.3dbody.tech/cap/abstracts/2017/17192ahmad.html

48. Kowalski M, Naruniec J, Daniluk M. Livescan3D: A Fast and Inexpensive 3D Data Acquisition System for Multiple Kinect v2 Sensors. In: 2015 International Conference on 3D Vision. 2015. p. 318–25.

49. Yang L, Zhang L, Dong H, Alelaiwi A, Saddik AE. Evaluating and Improving the Depth Accuracy of Kinect for Windows v2. IEEE Sens J. 2015 Aug;15(8):4275–85.

50. Lachat E, Macher H, Mittet MA, Landes T, Grussenmeyer P. First experiences with Kinect v2 sensor for close range 3D modelling. The International Archives of Photogrammetry, Remote Sensing and Spatial Information Sciences. 2015;40(5):93.

51. Wicke J, Dumas GA. Influence of the volume and density functions within geometric models for estimating trunk inertial parameters. J Appl Biomech. 2010 Feb;26(1):26–31.